Available online at www.sciencedirect.com
SCIENCE DIRECT®
Advances in Water Resources 26 (2003) 609–622
Advances in Water Resources
www.elsevier.com/locate/advwatres

Prediction of interfacial areas during imbibition in simple porous media

M. Gladkikh [a], S. Bryant [b,*]

[a] The University of Texas at Austin, Texas Institute of Computational and Applied Mathematics, 1 University Station CO200, Austin, TX 78712-0227, USA

[b] Department of Petroleum and Geosystems Engineering, The University of Texas at Austin, 1 University Station CO300, Austin, TX 78712-0228, USA

Received 22 November 2002; received in revised form 12 February 2003; accepted 5 March 2003

Abstract

The interfacial area between wetting (W-) and non-wetting (NW-) phases is one of the crucial parameters in several flow and transport processes in porous media. This paper gives predictions of such areas during imbibition (displacement of NW-phase by W) in simple porous media. The total interfacial area includes contributions from thin films of W-phase around soil particles, from trapped volumes of NW-phase, and from the meniscus between bulk NW- and W-phases. Imbibition was simulated with simple but physically representative pore-scale calculations in a geometrically predetermined random sphere packing. This approach allows the prediction of interfacial areas for different initial conditions (arising from different drainage endpoints, for example) and the investigation of the influence of phenomena such as "snap-off" of NW-phase due to coalescence of pendular rings. We find that the trend of interfacial area as a function of saturation is not sensitive to these considerations. These predictions were compared to different experimental data and were consistent with most of them. The predictions are also consistent with the conditions imposed by thermodynamics.

Keywords: Interfacial area; Porous media; Imbibition; Finney packing; Snap-off; Network model

1. Introduction

The interface between *wetting* (W-) and *non-wetting* (NW-) phases controls many transport process in porous media, such as contaminant flow, adsorption or dissolution. Thus, the knowledge of the area of such interface is important for modeling these transport phenomena.

There exist different methods and techniques which give the estimates for interfacial areas. They include direct measurements of the interfacial area between W- and NW-phases [30], but this is rather difficult to employ. Emerging technologies, such as magnetic resonance imaging [17] and indirect methods, such as the interfacial tracer technique [9,21,34,35] and a surfactant technique [19] allow obtaining experimental data for interfacial areas. A thermodynamic approach [3,23,30,31] estimates areas from measurements of capillary pressure curves. Different soil models (e.g. [15,20,25,32] give predictions for such areas. Also the digitization of the pore space or its images can be used in conjunction with models of fluid configuration for calculations of interfacial area [1,7].

Results to date from these techniques exhibit considerable variation in the trend of area versus saturation and in the magnitude of the areas. To obtain an independent assessment of these trends, we have undertaken a theoretical investigation in a simple but physically representative model porous medium. The model is a random packing of spheres for which the coordinates of the centers have been measured [10]. Knowledge of the coordinates determines the grain space and the void space in the packing, thereby overcoming a long-standing difficulty for theoretical approaches. Mason and Mellor [26] first used this model porous medium to investigate imbibition, and the work presented here follows their approach. Although a network representation of pore space is used for numerical calculations, this approach differs from many network models in that the features of the network are extracted directly from the geometry of the model porous medium.

* Corresponding author. Tel.: +1-512-471-3250.
E-mail addresses: mgla@ticam.utexas.edu (M. Gladkikh), steven_bryant@mail.utexas.edu (S. Bryant).

0309-1708/03/$ - see front matter © 2003 Elsevier Science Ltd. All rights reserved.
doi:10.1016/S0309-1708(03)00034-4

Despite the simplicity of the model porous medium, it is a powerful tool for investigation of the processes which occur in porous media. In particular it allows a priori predictions of macroscopic behavior (e.g. [4–6]) that have been validated by experimental data.

The purpose of this paper is to predict the interfacial areas during imbibition process in the Finney packing, which is physically representative of simple soils, and investigate the influence of several effects, which may take place during this process.

2. Pore-scale model of porous media

Different types of natural porous media almost always have very complicated pore space geometry, which is very hard to model. Even for unconsolidated grains, the pore space is irregular and cannot be described analytically. A network or lattice of sites connected by bonds qualitatively captures the essential features of the pore space in a granular medium. Assigning quantitative attributes such as coordination number, pore throat sizes, pore body sizes, etc. to the network is not straightforward, however. The usual approach for geometric attributes is to sample a frequency distribution. Mason [27] proposed a different approach, based upon extracting a network model of pore space from a geometrically predetermined random sphere packing.

In order to obtain such a network model, one must define "sites" and "bonds" of the network. For this purpose the Delaunay tessellation is used, which subdivides a set of points by grouping four nearest neighbors together. Applied to the sphere centers of the Finney pack, this procedure subdivides the volume of the packing into tetrahedral cells (Fig. 1).

Thus, a simple network is built (Fig. 2): its "sites" (*pore bodies*) correspond to tetrahedral Delaunay cells and its "bonds" (*pore throats*) correspond to the faces of those cells. All geometrical features of these pore bodies and throats (such as their volume, area etc.) follow directly from the known coordinates of the sphere centers.

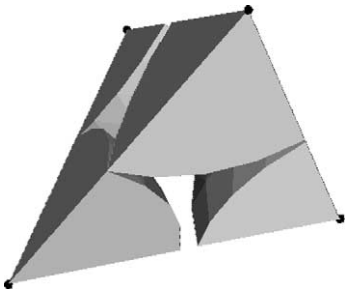

Fig. 1. Tetrahedral cell within the Finney pack, resulting from Delaunay tessellation. The apices of the tetrahedron are the centers of four nearest neighbor spheres. Only the sections of the spheres contained within the tetrahedron are shown.

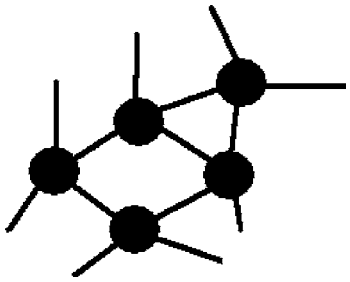

Fig. 2. Schematic representation of a network model. The circles correspond to tetrahedral cells, which are connected by bonds, which correspond to cell faces. Each site has four neighbors.

The topology of the network arises naturally: since each cell is a tetrahedron, it has four neighbors, resulting in a lattice of connectivity four. In this work the central 3367 spheres of the Finney pack were used, which yield a network with about 15,000 pores and 30,000 pore throats. More detailed description of the Finney pack and the network obtained from it by Delaunay tessellation can be found elsewhere [10,26,27].

3. Model of imbibition

The configuration of two fluids in porous media is governed by the Young–Laplace equation, which relates capillary pressure to the curvature of the interface between two phases:

$$P_c = \sigma C \tag{1}$$

where $P_c = P_{nw} - P_w$ is the pressure difference between W- and NW-phases; σ is the interfacial tension between them and C is the curvature of the interface. For simplicity we assume also that the solid grain surfaces are wetted perfectly, so the contact angle is zero. (The influence of the wettability on interfacial area during imbibition will be the subject of future investigations.) In spite of the fact that Eq. (1) describes a static configuration, it is commonly applied to the displacement of one immiscible phase by another, when that displacement occurs sufficiently slowly for capillary forces to dominate.

In our simulations, the process of imbibition starts from the end-point of primary drainage, where irreducible W-phase saturation is obtained. It is assumed for the simplicity of calculations that at this starting point W-phase in porous medium exists only as *pendular rings* (Fig. 3) around *grain contacts*. (In this work, a grain contact is a pair of neighboring spheres, which need not actually touch. W-phase supported within the gap between two spheres is often called a *liquid bridge*; for brevity we use the term "rings" to refer to liquid bridges as well.) Pendular rings always exist when two spheres actually touch. If a gap separates the two

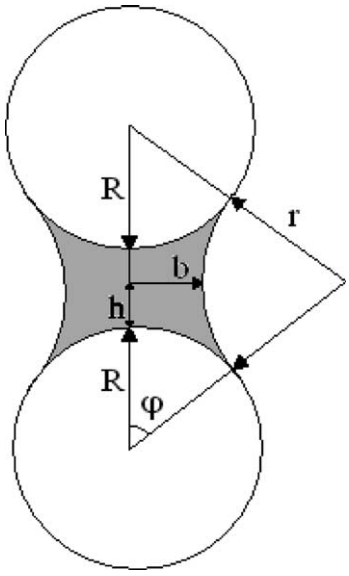

Fig. 3. Pendular ring around grain contact as a body of revolution with two principal radii: liquid neck b and r.

spheres, a pendular ring can exist only at curvatures below a critical value that depends upon the gap between spheres. The geometry of such rings will be discussed below in more detail. Then, from this starting point on, the curvature of the interface decreases, which allows W-phase saturation to increase. (Experimentally, a reduction in curvature is achieved by reducing the capillary pressure, Eq. (1), and we use these terms interchangeably.) W-phase is able to invade a pore body only if the current curvature of the interface is less than a certain *critical curvature* that depends upon the geometry of that pore. The first attempt to define this critical curvature was made by Haines [14] as

$$C_{\text{in}} = 2/R_{\text{in}} \tag{2}$$

where R_{in} is the radius of the sphere inscribed into the pore body (such a sphere would touch each of four pore grains). This so-called *Haines insphere curvature* would allow negative hysteresis for some pores, that is, their critical curvature for drainage would be less than the critical curvature for imbibition [26]. In order to avoid this non-physical effect, Mason and Mellor proposed to use *imbibition curvature* instead:

$$C_{\text{imb}} = C_{\text{in}} - 1.6/R_{\text{grain}} \tag{3}$$

where R_{grain} is grain radius. We adopt this as the definition of critical curvature for imbibition.

In order to simulate imbibition, it is also necessary to define entrance and exit pores. The entrance pores are assumed to be always connected with the W-phase reservoir, and through them W-phase will invade the packing. The exit pores are assumed to always be connected with the NW-phase reservoir, and through them displaced NW-phase will leave the packing. The pores that are actual surface pores of the Finney pack are natural choices for entrance and exit pores. However, Mason and Mellor [26] have shown that the Finney pack has a high ratio of surface pores to internal pores in comparison with real samples. Consequently simulations in which a large fraction of the surface pores are taken as W-phase entrances do not give a sharp *percolation threshold* (that is, sudden invasion of a large volume of the sample, once the curvature reaches a critical value). In order to replicate the percolation behavior of real samples, Mason and Mellor proposed to diminish the number of entrance cells. Using this technique, they obtained percolation threshold at the dimensionless (i.e. for grain radius equal to 1) curvature about of 4.1, which is close to the values observed during experiments. In the calculations presented in this paper, the number of entrance pores was 6 of the 1959 actual surface pores, which gave the same threshold curvature of about 4.1. As for exit pores, taking them to be actual surface pores does not contradict physical considerations. The influence of different choices for exit pores (e.g. some fraction of the surface pores, a random selection of pores from within the packing, etc.) on the residual NW-phase saturation is interesting, but is beyond the scope of this paper.

The algorithm for imbibition is based on the implementation described in [26]; we have extended it to account for trapping of the NW-phase. The algorithm proceeds by diminishing the current (global) dimensionless curvature by a small value (in the simulations performed in this paper the decrement in dimensionless curvature was 0.1). A pore containing NW-phase is a candidate for imbibition if it is the neighbor of one or more already imbibed pores or if there is W-phase in any throat of that pore. The latter condition only applies to pairs of non-imbibed cells. It can arise as the result of *coalescence of pendular rings* (this effect will be discussed below). Each candidate for imbibition is checked to determine whether it is contained in a cluster of pores connected to an exit pore. The existence of such a cluster implies a continuous path of pores containing NW-phase from the candidate pore to the NW-phase reservoir. If this condition is not met, the pore is removed from the list of candidates; the pore and other pores containing NW-phase that are connected to it are added to the list of pores containing *entrapped NW-phase*. (Alternative entrapment strategies will be described below.) Everything within a trapped cluster becomes frozen, in the sense that all pendular rings and menisci within the cluster will not change or move. This is because we assume incompressibility of NW-phase, so the interface of trapped cluster cannot change with the decrease of capillary pressure. Once the trapped pores are labeled, the remaining candidates are tested to see which will be imbibed. If the current curvature is less than the imbibition curvature of a candidate for imbibition, then

this pore will be imbibed. Newly imbibed cells are removed from the list of candidates, and this list is rechecked as described above. When no more cells can be imbibed, it means that an equilibrium configuration has been reached at the current curvature. At each value of the current curvature, it is also necessary to check pore throats for *snap-off* (coalescence of pendular rings) and to calculate the areas and volumes of menisci and pendular rings. This completes one iteration of the algorithm, and the current curvature can be diminished again. This algorithm works well for small decrements of curvature, and several key features of the resulting imbibition curve are in good agreement with experiments [26].

4. Pendular rings and their coalescence

As pointed out above, it is assumed that at the starting point of imbibition W-phase exists only in the form of rings around grain contacts. Moreover, it is assumed that these rings have toroidal form, that is, they can be considered as a body of revolution with circular cross-sections (Fig. 3).

On this figure a pendular ring is shown between two equal spheres of radius R separated by a gap of $2h$. This ring has radii of curvature b and r in its two principal directions. The curvature of the toroid is approximated by $C = 1/r - 1/b$. This simple approach was described by Haines [13] and allows one to obtain formulas for all necessary features of the ring (such as its volume and surface area) as a function of the curvature from geometrical calculations. Such formulas for $h = 0$ can be found, for example, in [12,28,33] and for $h > 0$ in [18].

The true form of the ring is not toroidal, but can be found from the fact that its surface must have constant curvature everywhere. The latter condition produces a surface known as the *nodoid*. Obtaining the features of such a body is not simple and demands numerical solution of differential equations. For the case $h = 0$ these calculations were thoroughly made by Fisher [11], who has found errors due to simplified toroidal approximation, and later by others such as Erle et al. [8] and Lian et al. [24]. According to Fisher, at small values of W-phase saturation (angle φ (cf. Fig. 3)) is about 10–20°), the error in liquid neck b is about 1–2% and in volume 3–5%. This range of values of φ corresponds to relatively high curvatures and, thus, to the beginning of imbibition, when most of the W-phase is in this form. These errors increase by a factor of four at high saturation (angle φ is about 40°, which corresponds to very low curvature, and, thus, to the final stages of imbibition, when there are almost no rings remaining in the pore space). From this analysis we conclude that the toroidal approach is sufficiently accurate when the contribution to the W-phase saturation and interfacial area from such rings is significant. Thus, this approximation can be used in the imbibition calculations.

In a dense packing of equal spheres, the average sphere has approximately eight contacts that will support pendular rings [2]. The presence of multiple rings on a single sphere raises the possibility of *coalescence* as the volume of the rings increases during imbibition. This effect was thoroughly analyzed by Haines [14] and is often called snap-off of NW-phase in pore throats, because it leads to full closure of pore throats (bonds of the network—faces of tetrahedral cells) with W-phase. The stages of coalescence of pendular rings are shown in Fig. 4.

Consider three spherical grains, which are in point contact with each other. There will be three pendular rings at the grain contacts. With decreasing curvature (and, thus, increasing W-phase saturation) pendular rings grow and at some point they will touch each other (Fig. 4a). As pointed out above, each pendular ring has two principal radii of curvature: one is convex (liquid neck) and the other is concave. Now consider the changes within the system as the W-phase saturation is further increased. In the narrowest part of the pore throat additional W-phase would necessarily occupy more of the void space, thereby diminishing the diameter of the pore throat occupied by NW-phase. Consequently, the concave curvature of the interface would increase. To maintain a surface of constant curvature the convex curvature of rings would also has to increase. This can only happen if the radius of the liquid neck *decreases*, which is inconsistent with an *increase* in W-phase saturation. This contradiction is resolved by filling the pore throat with W-phase, causing snap-off of the NW-phase. At this final stage of coalescence the pore throat is full of W-phase, which is shown in Fig. 4b, and the previously continuous volume of NW-phase now exists in two distinct blobs (not shown).

Using the toroidal approximation of the ring geometry described above, it is straightforward to obtain the *coalescence curvatures* for each pore throat in the packing, i.e. curvatures at which neighboring pendular

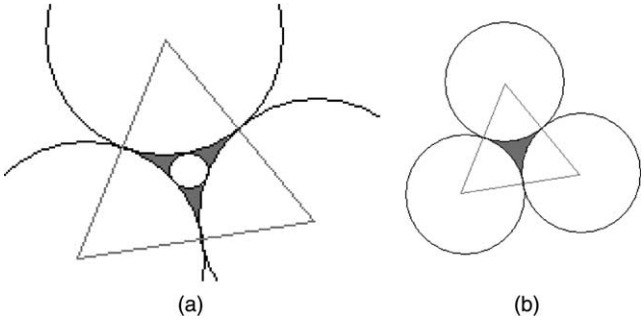

Fig. 4. (a) Initial stage of coalescence. Three pendular rings just touch each other. (b) Final stage of coalescence. Pore throat is full of W-phase.

rings will coalesce. Not all throats in the model porous medium are formed by three spheres in contact. The mutual disposition of these three spheres is different for each pore throat, which gives different coalescence curvatures for different throats. The distribution of such dimensionless coalescence curvatures in comparison with imbibition curvatures (obtained from Eq. (3)) is shown on Fig. 5.

Since coalescence of pendular rings leads to the closure of pore throats to NW-phase, it diminishes NW-phase connectivity and so not only increases W-phase saturation, but also increases the likelihood of entrapment of NW-phase. This qualitative argument has led to the conventional wisdom that these snap-offs are one of the key features of the imbibition process and strongly affect the value of residual NW-phase saturation. But the calculations presented below show that the influence of snap-off in a bead pack is almost negligible. This is readily explained by the lesser values of coalescence curvatures in comparison with imbibition curvatures, as can be seen in Fig. 5. By the time the capillary pressure (current curvature) has been reduced enough to initiate coalescence, much of the packing has already been imbibed. (Recall that percolation occurs at a dimensionless curvature of about 4.1.) These results will be explained below in more detail.

Finally, we consider two extreme cases of W-phase connectivity. In the first case W-phase is connected throughout the whole packing, i.e. pendular rings throughout the packing grow and change their shape simultaneously with the decreasing of curvature. Physically, this case corresponds to imbibition over time scales large enough for bulk volumes of W-phase to flow from the W-phase entrance pores to the rings through films on grains. In the second case W-phase is assumed to be connected only in the immediate vicinity of the meniscus between connected NW- and W-phases. This means that only pendular rings that are neighbors of imbibed pores can grow as curvature is decreased. This corresponds to shorter time scales, over which film flow across more than one grain is negligible. The difference between these two extremes will be discussed below.

5. Entrapment of NW-phase

During imbibition, NW-phase can be *trapped* inside the pore bodies, which results in the *residual NW-phase saturation* at the end of the process (at zero curvature of bulk W-phase). The value of this residual saturation is itself very important and demands separate discussion. NW-phase can be trapped in one pore body or in several neighboring pore bodies (*trapped cluster of pores*) due to the loss of connectivity with the exit pores, i.e. with the pores assumed to be connected to the NW-phase reservoir. On Fig. 6 one possible way of entrapment of NW-phase is represented. In this figure W-phase is shown by grey color and NW-phase by black. In configuration I the central and lower pores are not imbibed yet and contain NW-phase. Suppose that the lower cell has an

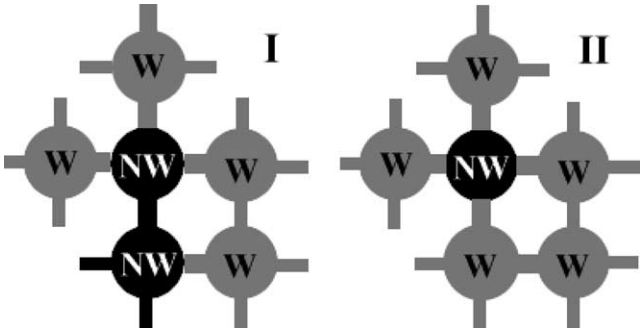

Fig. 6. One of the possible ways of entrapment of NW-phase. The lower NW-phase containing pore has a higher critical imbibition curvature than the middle NW-phase containing pore. Thus it imbibes first, in this case with the meniscus advancing from the pore, containing W-phase, at the bottom right. The meniscus cannot continue its advance into the middle pore, because the critical imbibition curvature for the middle pore is smaller. Thus the NW-phase in the middle pore is trapped.

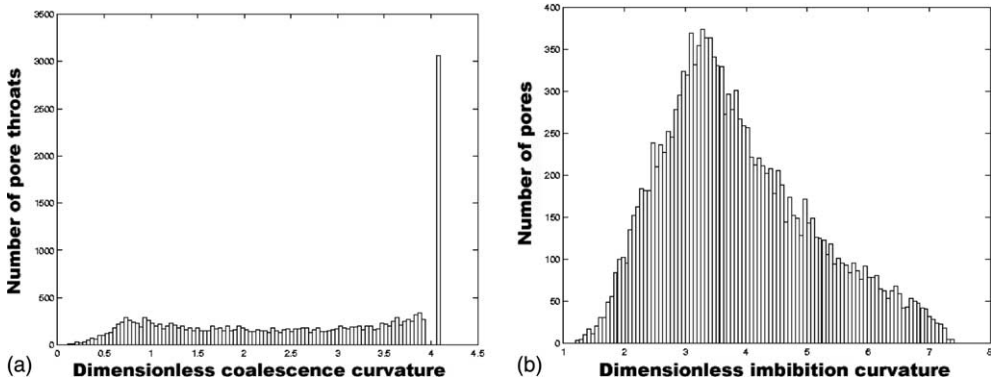

Fig. 5. (a) Distribution of dimensionless coalescence curvatures. The peak at $C = 4.1$ corresponds to coalescence in throats formed by three spheres in contact. (b) Distribution of dimensionless imbibition curvatures in the Finney packing.

exit pore as a neighbor, so NW-phase in configuration I is connected to the NW-phase reservoir and thus is not trapped. Suppose further that the lower pore has a higher imbibition curvature than the central pore and is connected to some other pore containing W-phase, in this case the pore at the bottom right of the figure. Then as the capillary pressure is reduced, the lower pore will imbibe first, and at that moment the central pore loses its connection to the NW-phase reservoir and becomes trapped.

This simple explanation allows constructing several computational strategies for entrapment.

The strategy of defining certain pores as the exits for NW-phase was described above. The residual NW-phase saturation obtained using this strategy will depend upon the number and spatial distribution of the exits. For example, taking the actual surface pores of the packing as exits results in a residual NW-phase saturation of about 20% of pore volume. Choosing the same number of pores randomly distributed throughout the whole packing results in a residual saturation of 10%. This is because the average distance to an exit pore is smaller in the latter case.

Experimental studies of the morphology of residual NW-phase suggest that most trapped clusters of NW-phase span only a few pores. This suggests that the average distance to an exit pore is rather small. Thus an alternative strategy for simulating entrapment is to invoke a predetermined value of *maximal possible cluster size*. That is, clusters of NW-phase larger than this threshold are assumed to be connected to the NW-phase reservoir and thus cannot be trapped, while smaller clusters are assumed to be disconnected. As a surrogate for the size of a cluster in space, we use the number of pores in the cluster. The results of the implementation of such a strategy depend on the maximal allowed cluster size, although the frequency distribution of small clusters (three pores or fewer) is remarkably similar for a wide range of maximal sizes. While the physical basis for this strategy is at best qualitative, it is computationally much cheaper and is useful for comparison with other strategies. It should be emphasized here that while the choice of strategies significantly affects the residual NW-phase configuration, it has very little effect on the calculated areas and volumes. The detailed analysis of NW-phase entrapment and structure of residual NW-phase will be the subject of future publications.

6. Computation of meniscus areas and volumes

When an imbibed pore adjoins a non-imbibed pore, W-phase occupies the face (pore throat) that connects these pores and forms a meniscus within the non-imbibed pore. This meniscus can intersect pendular rings and other menisci as well, and the geometry of this complex configuration is defined by the fact that its surface must have constant curvature. However, exact calculations of the area and volume of such a surface are very complicated. We have implemented a greatly simplified estimate instead. The meniscus is assumed to have locally spherical form within the cell (Fig. 7).

When the meniscus enters a pore (as a result of imbibition of a neighboring pore or of coalescence in a throat), it is assumed to immediately occupy a fixed position and shape within the pore. Subsequent changes in current curvature are ignored. The fixed position is calculated as follows: the meniscus is assumed to occupy the place between the three spheres, which define the pore throat (face spheres with the centers A, B and C (Fig. 7b)) and the sphere inscribed into the pore (with the center O on Fig. 7) and having radius R_{in} (the same

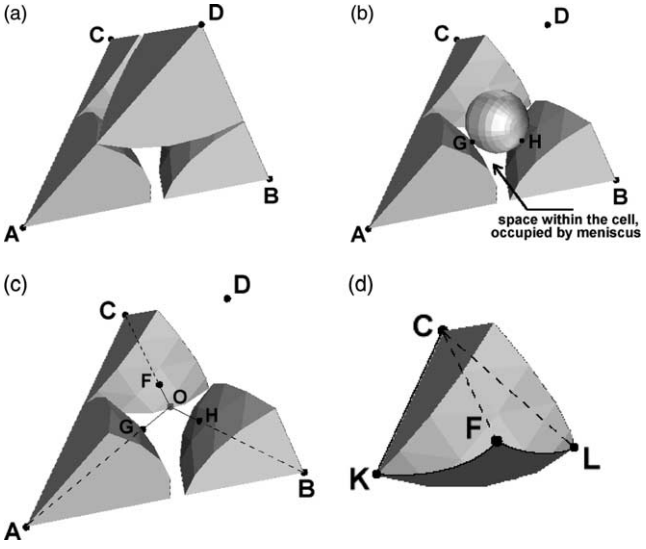

Fig. 7. (a) A pore in the Finney pack, corresponding to a tetrahedral cell determined by Delaunay tessellation. A, B, C and D—centers of four nearest neighbor grains, which are the vertices of the cell. (b) Simplified estimate of meniscus geometry. Upper sphere with center D on (a) has been removed to reveal the inscribed sphere within the pore, which touches all four grains. A, B and C—centers of grains (face spheres). G and H—points of contact between the inscribed sphere and corresponding grains. Vertices A, B and C define a pore throat. W-phase has imbibed into the pore below the plane ABC, while the pore above still contains NW-phase. The resulting meniscus is assumed to occupy the space within the latter pore under the inscribed sphere. (c) The sub-tetrahedron ABCO, corresponding to the face occupied by W-phase, is used to define the upper extent of the meniscus. The inscribed sphere, which is shown in (b), is removed. F: point of contact between the inscribed sphere and the grain centered at C. O: center of the inscribed sphere. (d) To estimate the area of face sphere centered at C in contact with the W-phase, we use the solid angle formed at vertex C by edges CA, CB and CO. These edges connect C with the two other grain centers (A and B) and the center of the inscribed sphere O (cf. c). Points K, L and F are the points where the edges CA, CB and CO intersect the grain surface. The surface of contact between the grain and meniscus is that part of a grain surface subtended by the solid angle (triangle KFL on the surface of the grain, shown in the picture by a darker color). Pendular rings at grain contacts K and L are not shown for clarity.

as in Eq. (2)). The W-phase volume is bounded by the face ABC of tetrahedral cell from below, by part of the inscribed sphere from above and by the face spheres from each side (Fig. 7b). The extent of the meniscus into the pore is taken to be the plane containing the points of contact (G, H and F in Fig. 7b and c) between the inscribed sphere and the face spheres. The main error introduced by this approach is neglecting the growth and advance of the meniscus inside the pore as the curvature decreases. On the other hand, this approximation eliminates the difficult problem of computing the intersection of menisci inside a pore. This is because the approximation restricts the meniscus location into non-overlapping subdivisions of the pore. That is, the pore is subdivided into four sub-tetrahedra (Fig. 7c) corresponding to the cell faces, with the vertices in the face sphere centers and the center of the inscribed sphere (sub-tetrahedron ABCO on Fig. 7). When the meniscus advances into the pore from the face, it is restricted by faces of the sub-tetrahedron and so cannot intersect other menisci. In the extreme case of four menisci inside a single pore, the NW-phase will occupy the inscribed sphere within the pore. The intersection between meniscus and pendular rings cannot be avoided even in this simplified approximation, which therefore overestimates the area of contact between W-phase and grain surfaces. The local error due to such intersections is large only at small curvatures (at the end of imbibition) when the number of such intersections is small, and thus its effect on the computed total interfacial area is relatively minor.

The calculations of meniscus volume and surface area are straightforward. The volume can be found in the same fashion as a pore body volume, that is, as a volume of the appropriate sub-tetrahedron (ABCO on Fig. 7), minus volumes of face spheres and the inscribed sphere, which are contained within this tetrahedron. The surface area of the meniscus can be found as an area of that part of inscribed sphere surface below the plane of contact with the face spheres (plane GHF in Fig. 7c). The area of contact between the meniscus and face spheres can be found using appropriate solid angles. For example, the solid angle at vertex C formed by segments CA, CB and CO subtends a spherical triangle KFL on the surface of grain C, and this is taken to be the surface in contact with W-phase. Similar constructions are applied at vertices A and B. For a coalescent face (pore throat) between two non-imbibed pores, the pore throat itself will contain W-phase, and two menisci will be formed, one within each pore. They can be treated exactly the same way as described above. The difference is only in the nature of their origin.

This simplified approach of meniscus calculations introduces errors, but they are significant mainly at the beginning of imbibition. Because the meniscus is assumed to reach its maximal extent into the pore immediately, the approach clearly overestimates W-phase volume in the early stages of imbibition. The maximal error could be of order of 100% for some pores. The error is much less at later stages of imbibition, when the meniscus will have advanced much farther into the non-imbibed pores. These errors are primarily in the volume calculation; the area estimates are less sensitive to the meniscus location. Moreover, such errors do not change qualitative trends, influencing only on small details of obtained curves. The assumptions that lead to these errors are: locally spherical form of the meniscus within the pore, instant equilibrium of the meniscus and some numerical errors due to the simplified computation of the grain surface in contact with the meniscus.

7. Results

Simulations of the imbibition process in the Finney packing were conducted with the algorithms described above. We implemented several variations of connectivity assumptions and trapping criteria in order to study their effects on the process. In presenting the results we distinguish two contributions to interfacial area. One is the interface between bulk configurations of W- and NW-phase, i.e. menisci and pendular rings; the other is the interface between grain surfaces and NW-phase. The solid–NW-phase interface can be regarded as W–NW interface due to the presence of thin films around perfectly wetted solid particles. The role of such films in different transfer processes (and, thus, their behavior as a real interface) depends upon features such as their thickness (which determines whether contaminant particles could travel through them) and upon the time-scale of the processes. Clearly, the larger the time-scale, the more such films will contribute to transfer. The total interfacial area should therefore be considered as maximal possible interfacial area of the system.

The Figs. 8–11 depict total W–NW-phase interfacial area (curve III), which is the sum of the W–NW-phase interface (curve I) (corresponds to the bulk configurations, i.e. pendular rings and menisci) and the solid–NW-phase interface (curve II). Figs. 8 and 9 illustrate the effect of coalescence, and Figs. 10 and 11 show the effect of W-phase connectivity. There were six entrance cells for the simulations in Figs. 8 and 9 and 392 for Figs. 10 and 11. (A small number of entrance cells provide a ratio of surface to internal pores comparable to that found in natural samples [26], and consequently yields a sharp percolation threshold. Increasing the number of entrances broadens the percolation threshold but does not significantly affect the interfacial area.) As shown in Fig. 8, the total interfacial area decreases as W-phase saturation increases. At the beginning of imbibition, the W-phase saturation is about 3% of pore volume, and the dominant contribution to area is the

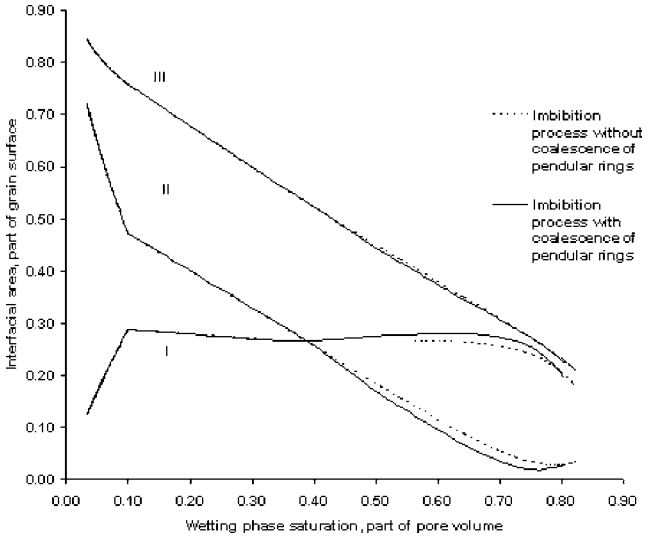

Fig. 8. Interfacial area and its components during imbibition process, normalized by total grain surface area. Effect of coalescence. I—area of bulk W–NW-phase interface, which is the sum of pendular rings and meniscus areas (curves IV and V in this figure correspondingly); II—area of solid–NW-phase interface (thin films of W-phase around solid particles); III—total W–NW interfacial area (sum of I and II components).

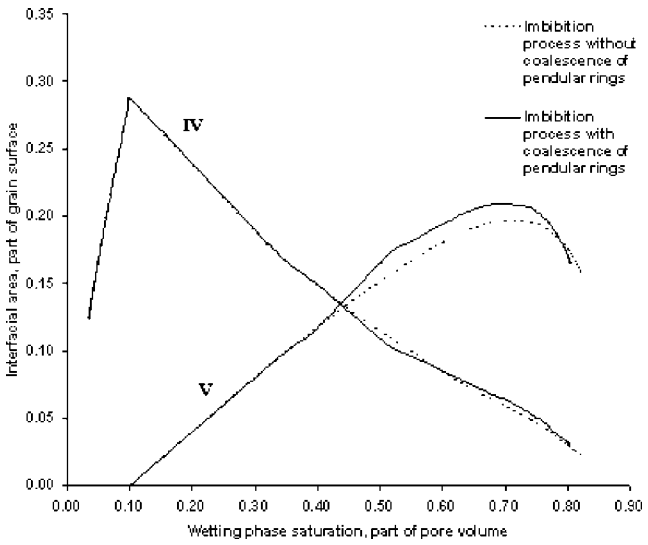

Fig. 9. Components of bulk W–NW-phase interfacial area (curve I on Fig. 8) during imbibition process, normalized by total grain surface area. Effect of coalescence. IV—area of pendular rings; V—area of menisci.

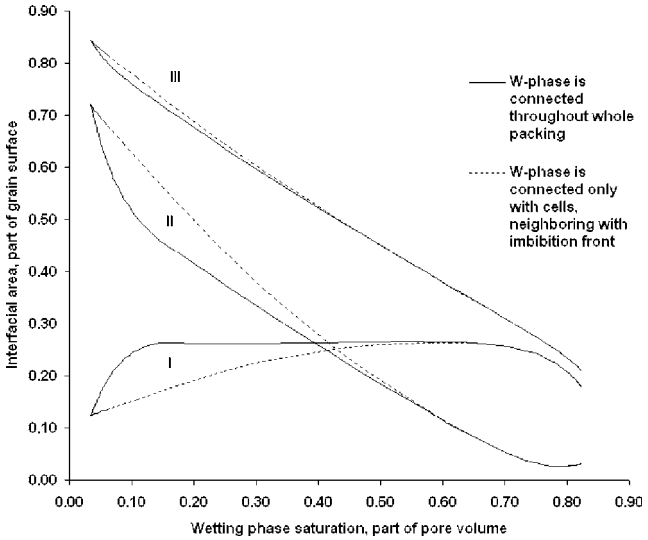

Fig. 10. Interfacial area and its components during imbibition process, normalized by total grain surface area. Effect of W-phase connectivity. I—area of bulk W–NW-phase interface, which is the sum of pendular rings and meniscus areas (curves IV and V on Fig. 11 correspondingly); II—area of solid–NW-phase interface (thin films of W-phase around solid particles); III—total interfacial area (sum of I and II components).

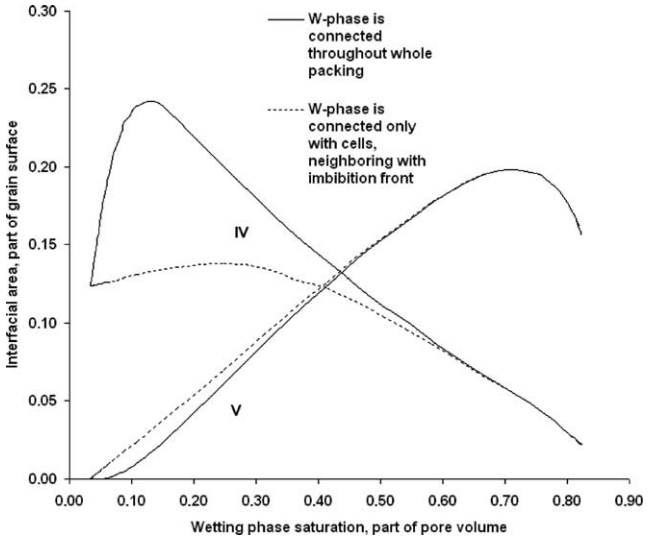

Fig. 11. Components of bulk W–NW-phase interfacial area (curve I on Fig. 8) during imbibition process, normalized by total grain surface area. Effect of W-phase connectivity. IV—area of pendular rings; V—area of menisci.

film on the grains. Despite their small volume, pendular rings cover almost 30% of the grain surface. The surface of the rings provides an area of the W–NW-phase interface. At the end of imbibition, the W-phase saturation is 80–90% of pore volume (this range of values was obtained from series of simulations, not presented here, using different entrapment strategies and W-phase connectivity) and the total area is 20–30% of the grain area. The dominant contribution is the area of residual NW-phase, which exists in the form of trapped blobs. The area of rings grows steadily at the beginning of imbibition because all W-phase is assumed connected; once the meniscus begins to advance into the pore space, the area of rings and menisci remains nearly constant. In contrast, the contribution of films diminishes steadily during the process as the number of pores containing

NW-phase decreases, with the exception of a slight increase at the end. This increase is very small in comparison with the values of other areas and is the result of our neglect of the mutual penetration of menisci and pendular rings.

Two components of this area are shown in Fig. 9: surface area of pendular rings (curve IV) and W-phase menisci (curve V). These components are not equal to zero at the end of the process, because both pendular rings and menisci become part of trapped clusters with NW-phase, and this area should be associated with the area of W–NW interface of such clusters with residual NW-phase. Of course, such subdivision could be done only at the first stages of imbibition, when rings and menisci exist independently of one another. At the end of the process W-phase forms one continuous body, where such rings and menisci coalesce and penetrate one into another.

On the Figs. 8 and 9, the influence of coalescence of pendular rings is presented. It was assumed in the literature before, that this effect of coalescence, or snap-off of pore throats, should be the defining feature of imbibition process and affect residual NW-phase saturation [16,22,29]. Our simulations indicate that in a bead pack, the influence of snap-off is almost negligible; affecting neither the qualitative behavior of the curves nor the residual NW-phase saturation (the difference is about 2–3%). This can be explained by the fact, that most pore throats will snap-off at dimensionless curvatures less than 4 (cf. Fig. 5), at which point almost all of the pores are already candidates for imbibition, and a significant fraction of the residual NW-phase has already been trapped. As a result, snap-off rarely creates new candidates for imbibition and so does not influence that process noticeably. Moreover, much of the reduction in local NW-phase connectivity accompanying snap-off occurs in volumes of NW-phase that would have been trapped anyway, so that snap-off affects residual NW-phase saturation only slightly.

The purpose of the calculations presented in Figs. 10 and 11 was to examine the influence of connectivity of W-phase on the total area and its components. Two extreme cases were considered. The solid curves are the results when the W-phase is assumed to be connected throughout the whole packing, so that all pendular rings grow simultaneously everywhere in the packing with each decrement in curvature. Under this assumption the endpoint of drainage (from which our imbibition simulations commence) should be zero W-phase saturation. The initial condition of 3% W-phase saturation in the simulations corresponds to W-phase held as pendular rings at grain contacts but no other W-phase present in the model porous medium (all pores are drained). Thus if connected to the W-phase source the pendular rings would shrink in response to an increase in capillary pressure, then reversibly expand when capillary pressure was reduced during imbibition. The curves in Figs. 10 and 11 do not show this reversible path between the origin (zero interfacial area at zero W-phase saturation) and the initial condition for imbibition.

The broken lines on Figs. 10 and 11 correspond to the assumption that a pendular ring adjusts its form in correspondence with the current curvature only if W-phase has advanced into one of the pores which contain this ring. To better illustrate the influence of these assumptions, the percolation threshold was softened by increasing the number of pores connected with the W-phase reservoir to 392; recall that in Figs. 8 and 9 there were only six such pores. The results on Figs. 10 and 11 show that the difference between these two extremes occurs only in the beginning of the process and represents the growth of rings in the first case before the penetration of W-phase inside the pack. At the end of imbibition the curves coincide. This means that there are no isolated pendular rings, i.e. rings that become trapped, when their form has not yet changed in accordance with current curvature of W-phase. This absence of isolated pendular rings is not trivial, but is confirmed by the analysis of pore-space during simulations. Other effects, such as choice of different entrapment strategies or diminishing the number of surface cells connected with W-phase reservoir, in order to obtain ratio of surface/internal cells close to real samples and achieve a sharp percolation threshold, also influence the process only slightly and do not change the qualitative picture of it.

These predictions for the interfacial area during imbibition are compared with experimental data from several sources in Fig. 12. The predictions were made with the following conditions: initial dimensionless curvature equals 10; pendular rings are connected with W-phase throughout the whole packing and their coalescence is allowed; number of cells, connected with W-phase reservoir is 6 (sharp percolation threshold); actual surface cells were taken as exits in order to define trapping criterion for NW-phase. It is also useful to estimate an upper bound for the area of solid in contact with the NW-phase. One bound comes from assuming that a non-imbibed pore contains no W-phase whatsoever, so that the entire grain surface within that pore is in contact with NW-phase.

In 1970 Morrow [30] measured area of residual NW-phase in random packing of 3-mm beads, using visual investigation of 2D-cross-sections after the phase configurations were ''frozen'' by in situ polymerization reactions. His value was 13.2% of total solid area. Unfortunately, he did not report his residual NW-phase saturation, so this result is plotted in the Fig. 12 as a line of constant value 0.132 of total solid area in the range of residual NW-phase saturations 0.1–0.2 of pore volume. Johns and Gladden [17] explored dissolution of octanol ganglia in random packings of glass ballotini and

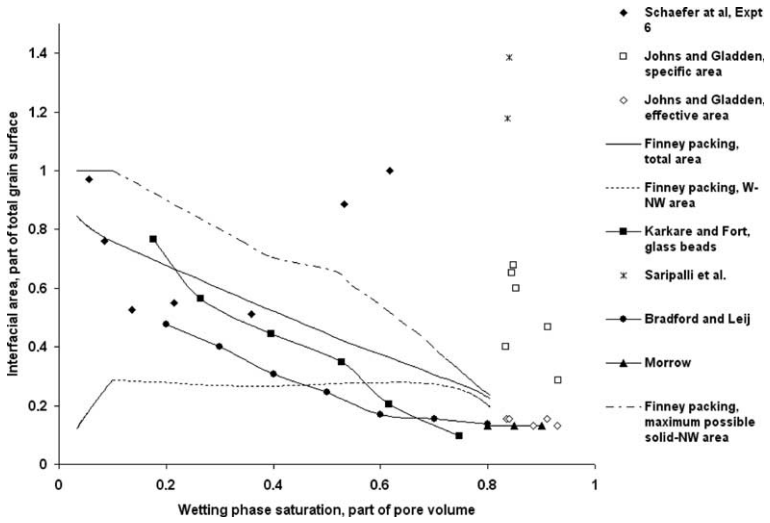

Fig. 12. Interfacial area and its components during imbibition process, normalized by of total grain surface area (coalescence is allowed, W-phase is connected throughout the whole packing, number of cells, connected with W-phase reservoir, is 6). Comparison with the experimental data.

measured residual NW-phase area by magnetic resonance imaging (MRI). They reported values of "specific" area, which corresponds to our total interfacial area (includes solid–NW interface), and "effective" area, which corresponds to the bulk W–NW-phase interface. For the former, they obtained values in the range from 0.3 to 0.7 expressed as a fraction of total solid surface; their residual NW-phase saturation ranged from 7% to 17%. For the latter, they reported values of about 0.15 for the same range of residual NW-phase saturation. These direct measurements of Morrow and values of effective area, obtained by Johns and Gladden, agree well with the predictions, given in this paper. As for the values of specific area, they represent the total interfacial area including solid–NW-phase area, so the difference between specific and effective areas is exactly the area of this solid–NW-phase interface. In some cases the values of these differences are about twice as large as maximal possible solid–NW-phase area for the Finney packing. The reason for this discrepancy remains puzzling, especially in light of the otherwise good agreement with predictions.

In 1996 Karkare and Fort [19] proposed a measuring technique based on the adsorption of insoluble surfactant. They measured air–water interfacial area as a function of W-phase saturation for both glass bead packings and sand columns, but they used preliminary interfusion of the sample with water–surfactant mixture, so their process was not equivalent to imbibition. As shown in Fig. 12, they obtained the same decreasing trend in the interfacial area, from about 0.8 of total solid surface area at low W-phase saturation to 0.1 at high saturations. Comparison with our predictions suggests that the solid–NW-phase area (thin films) is included in their measurements.

Bradford and Leij [3] computed interfacial area from imbibition data (capillary pressure vs. W-phase saturation) in an oil–air–sand system (oil wetted sand particles completely), based upon a thermodynamic approach [23,30]. For consistency with other data in the Fig. 12 the Bradford and Leij measurements have been normalized by the surface area of the mixture of sands used in their experiments, reported by them as 650 cm^{-1}. They also obtained a monotonic decrease in area. Their areas are smaller than our predictions, especially at the beginning of the process. This could be explained by the fact that they used mixtures of sands with a wide distribution of particle sizes, so that their irreducible W-phase saturation was larger than the value for our monodisperse packing. The interfacial area would be correspondingly smaller. Their residual NW-phase saturation was about 20% of pore volume.

This theoretical approach of Bradford and Leij (which was proposed for the first time by Leverett [23]) implies a linear relationship between the interfacial area and the area under the imbibition curve. Imbibition curves, obtained for different conditions in the Finney packing, are presented in Fig. 13. Imbibition corresponds to increase of W-phase saturation, so the free energy of the system must decrease during imbibition. At the same time the total surface energy must also decrease, implying that the total interfacial area must decrease. The loss of free energy corresponds to the work done in advancing the meniscus into the pore space and corresponds to the area under the imbibition curve. Our imbibition simulations permit independent calculations of this work and of the change in surface energy, and these are plotted against each other in Fig. 14. In Figs. 13 and 14 all values are dimensionless, i.e. for sphere radii equal to 1. Initial dimensionless curva-

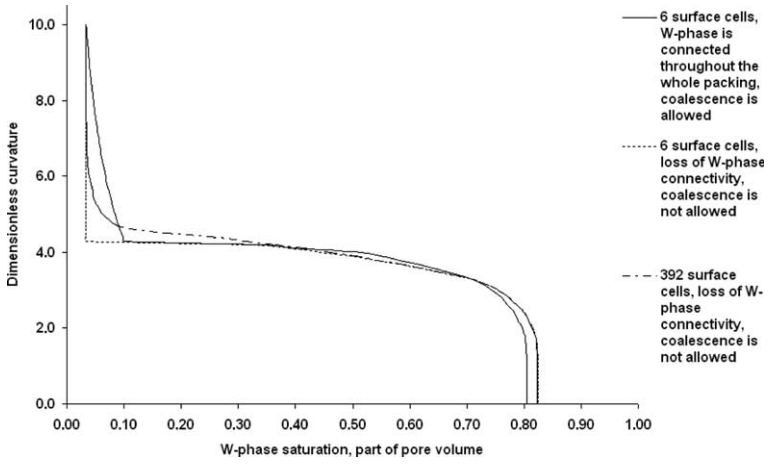

Fig. 13. Imbibition curves (dependence between dimensionless curvature and W-phase saturation) in the Finney packing.

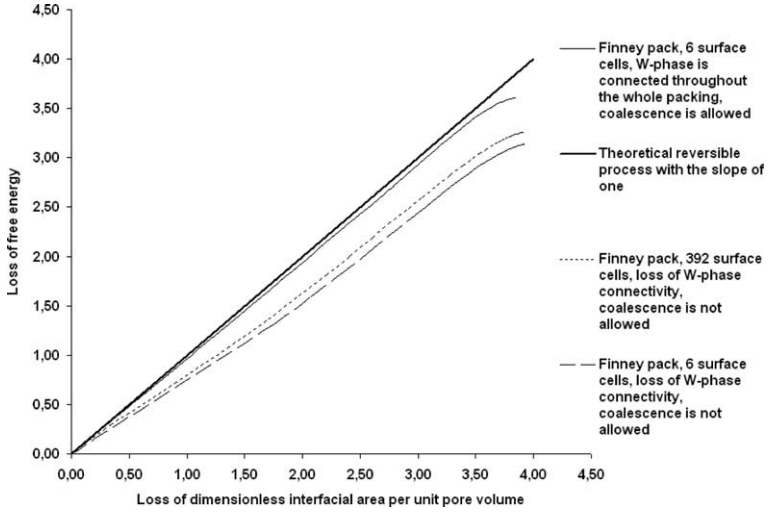

Fig. 14. Dependence between loss of the dimensionless free energy of the system and loss of its dimensionless interfacial area per unit pore volume during imbibition.

ture is equal to 10 in the calculations in Fig. 13 and to 50 for curves in Fig. 14. It is remarkable that the curve, obtained for assumptions with 6 surface cells and connectivity of W-phase, lies very close to the theoretical line, with the maximal discrepancy of about 7% at the end. Thermodynamic analysis assumes reversibility of the process, and thus the area under the imbibition curve represents the reduction in free energy during a reversible process. Imbibition, though, is not reversible (except for the case of pendular ring growth): there are losses of free energy (and, thus, of interfacial area) which occur during irreversible displacements (''rheons'' of Morrow [30]). Thermodynamic analysis does not take into account such displacements, and thus the path of a real process in Fig. 14 will have slope everywhere less than or equal to unity. All our simulations are consistent with this requirement.

Morrow [30] measured efficiency of imbibition as a ratio of work done by the system (which is equal to the area under the imbibition curve) to losses of free energy of the system due to destruction of interfaces (which can be determined from direct observation of interfacial areas). Obviously, losses of energy due to the irreversibility of the process can be found then as unity minus such defined efficiency. The comparison of such losses of energy as measured by Morrow to those computed from the presented simulations is shown in Table 1. As shown in this table, the magnitude of free energy loss due to irreversibility computed in our simulations compares well with Morrow's measurement. The assumption of W-phase being connected throughout the packing (i.e. pendular rings grow as curvature decreases) appears to approximate well the conditions of Morrow's experiment. The assumptions of poor W-phase connectivity

Table 1
Losses of energy due to irreversibility of imbibition

Imbibition conditions	Losses of energy due to irreversibility
Morrow's experiment	7.5%
6 surface cells, W-phase is connected throughout the whole packing, coalescence is allowed	6.2%
392 surface cells, loss of W-phase connectivity, coalescence is not allowed	14.8%
6 surface cells, loss of W-phase connectivity, coalescence is not allowed	20.1%

and the absence of coalescence produce larger values of the losses of energy due to the reversibility of the process, and so do not agree with the conditions of Morrow's experiment.

The thermodynamic consistency of the simulations presented in Fig. 14 and Table 1 is not trivial, because the relationship between area and volume differs significantly for different morphologies of phase configuration. For example, pendular rings have a surface to volume ratio of nearly 20, while the ratio for menisci is less than five, and the surface area of grains in contact with NW-phase has no direct relationship to saturation. (In contrast, consider a simulation that approximated phase saturation by the number fraction of pores occupied by that phase, and similarly approximated the interfacial area as a linear function of phase saturation. Such a simulation would trivially satisfy the thermodynamic relationship between imbibition curve and interfacial area.) From the above one can conclude that the phase configurations computed in the imbibition simulation are physically reasonable, and that the approximations in computations of the geometry of these configurations do not introduce substantial errors.

Schaefer et al. [35] and also Saripalli et al. [34] used similar interfacial tracer techniques and measured the interfacial area for imbibition in 0.335 mm silica sand [35] and different sands and glass beads packs [34]. They obtained results quite different from what was described above, Fig. 12. Schaefer et al. reported interfacial areas for some of their experiments (are not shown on Fig. 12) that were almost twice as large as total solid area at the beginning of imbibition. The reported area decreased more rapidly than our predicted trend, but the relative constancy for W-phase saturations between 0.13 and 0.4 is similar to the predicted W–NW area. They also reported an increase of area values toward the end of the imbibition process (W-phase saturations greater than about 0.5). An increase in *total* area would violate thermodynamics [23,30] though an increase in the bulk W–NW interface is conceivable if it were accompanied by a larger decrease in solid–NW area. Saripalli et al. measured the area of residual NW-phase, obtaining values from 1.2 to almost 8 times as much as total grain area for W-phase saturation of 80–0% of pore volume. Other researchers have reported similar results using this technique. Many measurements reported for drainage are also much higher than predicted [6]. The reasons for this are the subject of continuing investigation.

Overall, the predictions given in this paper provide reasonable values for interfacial areas and correctly describe the qualitative behavior of the system, which is verified by series of different experimental data, which were obtained with various techniques. It is interesting to compare these results with the predictions of Berkowitz and Hansen [1] in a geometrical model extracted from images of the pore space in a sample of Fontainebleau sandstone. They used a simulated annealing technique to find the minimum interfacial energy distributions at different saturations. Their calculated water–air and solid–air areas qualitatively match our bulk W–NW and solid–NW predictions. Moreover, their values for water–air area are in the range of 10–20% of total solid area, which agrees very well with calculations given in this paper.

It is remarkable also, that the assumptions regarding coalescence, W-phase connectivity and trapping criteria give only secondary corrections to the area values and do not change the general trend of the curves. If the contribution of thin films (solid–NW area) is included, the interfacial area curves decrease with W-phase saturation. If not, the interfacial area remains nearly constant during imbibition, because the decreasing number of pendular rings (and thus, their surface area) is roughly balanced by the increasing number of throats containing the meniscus. Thermodynamic considerations show that the monotonic decrease in *total* interfacial area is a necessary consequence of an imbibition curve that exhibits a monotonic relationship between capillary pressure and saturation. The two contributions to the total interfacial area need not be monotonic, however. The prediction of a roughly constant area between the two fluid phases indicates a remarkable degree of balancing across a wide range of saturations.

8. Conclusions

Using simple calculations on a geometrically predetermined random sphere packing, quantitative predictions of the interfacial area between W- and NW-phase during imbibition process were made. Two important phenomena, connectivity of W- and NW-phase trapping, were treated by considering physically reasonable limiting cases. Remarkably, these phenomena affected the interfacial area curves only slightly. In particular, coalescence of pendular rings, or snap-offs, did not in-

fluence areas and only slightly affected residual saturations. This is because in this unconsolidated packing, the curvatures at which coalescence occurs are much lower than the curvatures at which most of the pore space is imbibed.

Though there are some errors due to simplifications in calculations (for instance, in meniscus areas and volumes), the predictions of the interfacial area are in a good agreement with different experiments. Data from [17,30] give quantitative results for the interfacial area of trapped "blobs" of residual NW-phase at the end of the process of imbibition, and these quantitative results confirm numerical predictions given in this paper. Also experiments from [19] and simulation from [1] together with theoretical approach of [3,23,30] verify the qualitative behavior of interfacial area during imbibition. The predictions are not consistent with other results, such as [32,34,35], but these results also exceed the total grain surface area considerably at some points and are sometimes non-monotonic. We have not been able to construct a plausible reconciliation of our model with these observations. It seems likely that other phenomena we have not considered in our model are influencing these measurements.

The predicted residual NW-phase saturations are also in good agreement with all experiments (about 15–20% of pore volume).

Overall, the analysis of Finney packing gives simple, but powerful tool for predictions of behavior of porous media during imbibition process. These predictions could be improved, for example, by providing more accurate values of imbibition curvatures of cells or more precise calculations of volumes and areas, which gives the directions for future work.

Acknowledgements

The research leading to the results described here has been supported by EPA (Science to Achieve Results (STAR) program, R827116/01/0) and with funds from the State of Texas as part of the program of the Texas Hazardous Waste Research Center (THWRC, 069UTA0803). The contents do not necessarily reflect the views and policies of the sponsor nor does the mention of trade names or commercial products constitute endorsement or recommendation for use. This research has not been subjected to any EPA review and therefore does not necessarily reflect the views of the Agency, and no official endorsement should be inferred.

References

[1] Berkowitz B, Hansen DP. A numerical study of the distribution of water in partially saturated porous rock. Transp Porous Media 2001;45:303–19.

[2] Bernal J, Mason J. Coordination of randomly packed spheres. Nature 1960;188:910–1.

[3] Bradford SA, Leij FJ. Estimating interfacial areas for multi-fluid soil systems. J Cont Hydr 1997;27:83–105.

[4] Bryant SL, Mellor DW, Cade CA. Physically representative network models of transport in porous media. AIChE J 1993;39:387–96.

[5] Bryant SL, Mason GJ, Mellor DW. Quantification of spatial correlation in porous media and its effect on mercury porosimetry. J Coll Int Sci 1996;177:88–100.

[6] Bryant SL, Johnson AS. Theoretical evaluation of the interfacial area between two fluids in a model soil. In: ACS Symposium Series. Chem Env 2001;806:26–41.

[7] Dalla E, Hilpert M, Miller CT. Computation of the interfacial area for two-fluid porous medium systems. J Cont Hydr 2002;56:25–48.

[8] Erle MA, Dyson DC, Morrow NR. Liquid bridges between cylinders, in a torus, and between spheres. AIChE J 1971;17:115–21.

[9] Faisal Anwar AHM, Bettahar M, Matsubayashi U. A method for determining air–water interfacial area in variably saturated porous media. J Cont Hydr 2000;43:129–46.

[10] Finney JL. Random packings and the structure of simple liquids. I. The geometry of random close packing. In: Proceedings of the Royal Society of London, Ser A. Math Phys Sci 1539;319:479–93.

[11] Fisher RA. On the capillary forces in an ideal soil; correction of formulae given by W.B. Haines. J Agric Sci 1926;16:492.

[12] Gvirtzman H, Roberts PV. Pore scale spatial analysis of two immiscible fluids in porous media. Water Resour Res 1991;27(6):1165–76.

[13] Haines WB. Studies in the physical properties of soils. II. A note on the cohesion developed by capillary forces in an ideal soil. J Agric Sci 1925;15:529–35.

[14] Haines WB. Studies in the physical properties of soils. IV. A further contribution to the theory of capillary phenomena in soil. J Agric Sci 1927;17:264–90.

[15] Held RJ, Celia MA. Pore-scale modeling extension of constitutive relationships in the range of residual saturations. Water Resour Res 2001;37(1):165–70.

[16] Jerauld GR, Salter SJ. The effect of pore-structure on hysteresis in relative permeability and capillary pressure: pore-level modeling. Transp Porous Media 1990;5:103–51.

[17] Johns ML, Gladden NF. Magnetic resonance imaging study of the dissolution kinetics of octanol in porous media. J Coll Int 1999;40:261–70.

[18] Johnson AS. Pore level modeling of interfacial area in porous media. MS Thesis, The University of Texas, Austin, 2001.

[19] Karkare MV, Fort T. Determination of the air–water interfacial area in wet "unsaturated" porous media. Langmuir 1996;12:2041–4.

[20] Kawanishi T, Hayashi Y, Roberts PV, Blunt MJ. Fluid–fluid interfacial area during two and three phase fluid displacement in porous media: a network model study. Int Conf and Special Seminars on Groundwater Qual: Remed and Protect Center for Groundwater Studies. Tubingen, Germany, 1998.

[21] Kim H, Rao PSC, Annable MD. Determination of effective air–water interfacial area in partially saturated porous media using surfactant adsorption. Water Resour Res 1997;33(12):2705–11.

[22] Lenormand R, Zarcone C. Role of roughness and edges during imbibitionin square capillaries. SPE 13264.

[23] Leverett MC. Capillary behavior in porous solids. AIME Pet Trans 1941;142.

[24] Lian G, Thornton C, Adams MJ. A theoretical study of the liquid bridge forces between two rigid spherical bodies. J Coll Int Sci 1993;161:138–47.

[25] Lowry M, Miller C. Pore-scale modeling of nonwetting-phase residual in porous media. Water Resour Res 1995;31:455–73.

[26] Mason GJ, Mellor DW. Simulation of drainage and imbibition in a random packing of equal spheres. J Coll Int Sci 1995;176:214–25.
[27] Mason GJ. A model of the pore space in a random packing of equal spheres. Colloid Interf Sci 1971;35:279.
[28] Melrose JC, Wallick GC. Exact geometrical parameters for pendular ring fluid. J Phys Chem 1967;71:3676–7.
[29] Mohanty K.K, Salter S.J. Multiphase flow in porous media: II. Pore level modeling. SPE 11018.
[30] Morrow NR. Physics and thermodynamics of capillary action in porous media. Ind Eng Chem 1970;40:32–56.
[31] Oostrom M, White MD, Brusseau ML. Theoretical estimation of free and entrapped nonwetting–wetting fluid interfacial areas in porous media. Adv Water Res 2001;24(8):887–98.
[32] Or D, Tuller M. Liquid retention and interfacial area in variably saturated porous media: upscaling from single-pore to sample-scale model. Water Resour Res 1999;35:3591–605.
[33] Rose W. Volumes and surface areas of pendular rings. J Appl Phys 1958;29(4):687–91.
[34] Saripalli KP, Rao PSC, Annable MD. Determination of specific NAPL–water interfacial areas of residual NAPLs in porous media using the interfacial tracers technique. J Cont Hydr 1998;30:375–91.
[35] Schaefer CE, DiCarlo DA, Blunt MJ. Experimental measurement of air–water interfacial area during gravity drainage and secondary imbibition in porous media. Water Resour Res 2000;36(4):885–90.